PERGAMON

Journal of Quantitative Spectroscopy & Radiative Transfer 63 (1999) 263–275

Journal of Quantitative Spectroscopy & Radiative Transfer

www.elsevier.com/locate/jqsrt

Light scattering properties of spheroidal coated particles in random orientation

Arturo Quirantes

Departamento de Física Aplicada, Facultad de Ciencias, Universidad de Granada, 18071 Granada, Spain

Abstract

We present results of light scattering properties for ensembles of randomly oriented, coated spheroidal particles with an equivalent-volume size parameter $kr_{eq} = 8$ and axial ratios $\varepsilon = 0.6{,}1$, and $1/0.6$. Müller matrix elements $F_{ij}(\theta)$ have been calculated using Waterman's T-matrix approach, as modified by Peterson and Ström for inhomogeneous particles, together with Mishchenko's orientation averaging procedure. Differences between oblate and prolate particles with the same short-to-long axis ratio, as well as between spherical and nonspherical scatterers, are outlined. Additional calculations for size parameters 1, 5 and 10 (not shown) have also been carried out for checking purposes.

Keywords: EBCM; Nonspherical coated particles; Müller matrix

1. Introduction

Many efforts have been made to extend the study of light scattering properties beyond Mie theory [1] for monodisperse, homogeneous spherical particles. Applications to polydisperse systems were then followed by the Aden-Kerker theory [2] for coated spherical scatterers. The next logical step — scattering by nonspherical particles — was taken in the form of a diversity of theories. One of them, Waterman's extended boundary condition method [3,4] (EBCM), also called the T-matrix method, has turned into one of the most powerful and efficient methods for scattering by nonspherical particles. Although it can be applied to virtually any kind of nonspherical particles, it is most efficient for axisymmetric scatterers, and Mishchenko [5] has developed an

E-mail address: aquiran@goliat.ugr.es (A. Quirantes)

0022-4073/99/$ - see front matter
PII: S0022-4073(99)00019-9

elegant and highly efficient method to extend a single-particle result to the case of particles in random orientation.

The T-matrix method has been extensively used for homogeneous particles (plus randomly oriented and/or polydisperse systems) [6]. But, considering that a T-matrix extension for coated and multicoated dielectric objects was given by Peterson and Ström [7,8] in 1974, the number of applications dealing with scattering properties of coated nonspherical systems using the EBCM has been rather small [9]. This might be due to the fact that T-matrix computations for coated, nonspherical particles can become both unstable and highly time-consuming, so that other methods can become more attractive, especially if no orientation averaging is necessary [10–13].

Still, the EBCM has showed its effectiveness in the study of nonspherical, axisymmetric particles in random orientation, and this feature can be exploited in an extension to coated particles. Real particle systems include pharmaceutical applications as drug carriers, studies of erythrocytes and magnetic materials for recording [14]. The possibility of evaluating the core of a composite particle with nondestructive methods makes light scattering a valuable tool as a probing and sizing technique.

In the present paper we intend to show the results of light scattering calculations for a suspension of randomly oriented, coated spheroids. We report results in the form of Müller matrix elements $\mathbf{F}_{ij}(\theta)$ for a range of relative core size and eccentricities. Due to the number of parameters involved (refractive indices, shape, outer and inner sizes), a wide range of sizes and shapes cannot be examined without enlarging the data volume to unacceptable levels, so we have restricted ourselves to the study of a single value of outer size kr_{eq} (where k is the wavenumber of light in the suspending medium and r_{eq} is the radius of the sphere with a volume equal to that of the particle), a single combination of refractive indices, and two values of eccentricity (three including the spherical case). While the results can obviously not be generalized to an arbitrary size, a comparison of data for different eccentricity values can yield some conclusions on the general behavior or light scattering properties with equal-volume particles. Comparison to additional data for size parameters $kr_{\mathrm{eq}} = 1$, 5, and 10 will help us to distinguish whether a particular scattering feature is characteristic to the particle size studied, or can be thought of as a more general light scattering property.

2. Theory

The so-called Müller, or scattering, matrix, describes the effect of a scattering volume on a light beam. The light beams of the incident and scattered radiation can be described by their Stokes vectors I_{i}, I_{s}; they are related to each other by means of the so-called Müller $\mathbf{F}$ matrix as

$$I_{\mathrm{s}} = \frac{C_{\mathrm{sca}}}{4\pi R^2}\,\mathbf{F}(\theta) I_{\mathrm{i}}, \tag{1}$$

where R is the distance between the scattering system and the detector, and C_{sca} its scattering cross section. Our goal is to calculate $\mathbf{F}$, which (together with cross sections) contains all available information about the angular variation of static light scattering properties. When the scattering system is composed of randomly oriented, axially symmetric particles in single scattering, the

Müller matrix has the following form [15]:

$$\mathbf{F}(\theta) = \begin{bmatrix} F_{11}(\theta) & F_{12}(\theta) & 0 & 0 \\ F_{12}(\theta) & F_{22}(\theta) & 0 & 0 \\ 0 & 0 & F_{33}(\theta) & F_{34}(\theta) \\ 0 & 0 & -F_{34}(\theta) & F_{44}(\theta) \end{bmatrix}. \tag{2}$$

In the first step of the calculation, the T-matrix is computed for a single particle in the so-called natural reference system (with the z-axis in the direction of the symmetry axis) [5]. For the case of a two-layered axisymmetric object (characterized by relative refractive indices m_1 for core and m_2 for shell), the T matrix is given by [7]:

$$\mathbf{T} = \begin{bmatrix} T^{11} & T^{12} \\ T^{21} & T^{22} \end{bmatrix} = -[\mathbf{B}_2 + \mathbf{BB}_2 \cdot \mathbf{T}_1] \cdot [\mathbf{A}_2 + \mathbf{AA}_2 \cdot \mathbf{T}_1]^{-1}, \tag{3}$$

where $\mathbf{T}_1$ is the transition matrix for the inner layer, as derived in the homogeneous case [7,9], but assuming refractive indices m_1/m_2, for the particle, and 1 for the medium, and an incident radiation wavenumber $k_o m_2$, where $\lambda_o = 2\pi/k_o$ is the vacuum incident wavelength. The matrices $\mathbf{B}_2$, $\mathbf{A}_2$ are such that $-\mathbf{B}_2 \cdot (\mathbf{A}_2)^{-1}$ is the T-matrix for the full particle, assumed homogeneous with refractive index m_2, and in a dispersion medium with refractive index equal to 1. In this case, the incident wave number is taken as k_o. Finally, the matrix $\mathbf{BB}_2$ is the same as $\mathbf{B}_2$, except that the Bessel functions of the first kind with argument kr are replaced by Hankel functions with the same argument; the same applies to the $\mathbf{AA}_2$ and $\mathbf{A}_2$ matrices.

In the second step of the process, the Müller matrix elements are expanded in a set of generalized spherical functions [16,17] $P^s_{mn}(\theta)$:

$$\begin{aligned} F_{11}(\theta) &= \sum_{s=0}^{\infty} a_1^s P^s_{00}(\cos\theta), \\ F_{22}(\theta) + F_{33}(\theta) &= \sum_{s=2}^{\infty} (a_2^s + a_3^s) P^s_{22}(\cos\theta), \\ F_{22}(\theta) - F_{33}(\theta) &= \sum_{s=2}^{\infty} (a_2^s - a_3^s) P^s_{2-2}(\cos\theta), \\ F_{44}(\theta) &= \sum_{s=0}^{\infty} a_4^s P^s_{00}(\cos\theta), \\ F_{12}(\theta) &= \sum_{s=2}^{\infty} b_1^s P^s_{02}(\cos\theta), \\ F_{34}(\theta) &= \sum_{s=2}^{\infty} b_2^s P^s_{02}(\cos\theta). \end{aligned} \tag{4}$$

Finally, the expansion coefficients a_i^s, b_i^s are related to the natural T-matrix elements [5]. Extinction and scattering cross sections can also be calculated from the T-matrix elements, if necessary.

In practical computations, the series expansion for the incident and scattered fields, in which the EBCM matrix is based [18,19], must be truncated after a finite number of terms n_{max}. This, in turns,

yields an upper value of $2 \times n_{\max}$ for Müller matrix element expansions (Eq. (4)), and limits the size of the T-matrix submatrices T^{ij} ($i,j = 1,2$; see Eq. (3)) to a size $n_{\max} \times n_{\max}$ each. Too high a value of $n_{\max}$ will result in instabilities in the matrix calculation process and an excess of computer usage; on the other hand, a value of $n_{\max}$ too low will prevent calculations from converging within the desired accuracy. The optimum number of terms $n_{\max}$ is established by calculating the values of C_1 ($= C_{\text{ext}}$, when the azimuthal number is set as $m = 0$) and C_2 ($= C_{\text{sca}}, m = 0$) until the relative differences of $C_1(n_{\max})$ and $C_1(n_{\max} - 1)$ are less than a given accuracy value Δ (same procedure for C_2).

However, we have two characteristic matrix sizes due to the existence of both core and shell, and this requires the calculation of two sets of matrices, whose size can be very different. This suggests the use of two of $n_{\max}$ values. A possible solution is to check the matrix size requirements for both the inner boundary (matrix $\mathbf{T}_1$ in Eq. (4)) and the outer boundary (matrices $\mathbf{A}_2$, $\mathbf{B}_2$, $\mathbf{AA}_2$, $\mathbf{BB}_2$), thus resulting in two $n_{\max}$ parameters: n_{mc}, n_{ms} for core and shell expansions, respectively. A similar criterion is used for light scattering calculations of coated spherical particles [15,20]; in accordance with it, we furthermore demand that $n_{\text{ms}} > n_{\text{mc}}$. Eq. (4) can be calculated by making $(T_1^{ij})_{nn'} = 0$ for $\text{Max}(n, n') > n_{\text{mc}}$.

Once the whole T-matrix (with T^{ij} size $n_{\text{ms}} \times n_{\text{ms}}$) is obtained, we can calculate the expansion coefficients and the $\mathbf{F}_{ij}(\theta)$ elements, whose series expansion goes from 0 (or 2, in some expansions) to $s_{\max} = 2 \times n_{\text{ms}}$. However, it is often not necessary to use all the T-matrix elements to calculate the expansion coefficients of Eq. (5) within the desired accuracy. Since the final calculations are roughly proportional to the fourth power of n_{ms} in both computer time and memory usage, it becomes convenient to substitute n_{ms} with $n_{\text{ms}2} < n_{\text{ms}}$ such that the use of $(T^{ij})_{nn'}$ elements with $n, n' < n_{\text{ms}2}$ will still yield a series expansion in Eq. (4) that converges to the desired accuracy. That is, n_{ms} is used to accurately obtain the T-matrix, while $n_{\text{ms}2}$ is used to calculate cross sections and Müller matrix elements. This procedure requires a negligible programming effort and speeds up the computations.

The convergence in N_{g} (the number of Gauss quadrature points for the calculation of matrix elements) is also calculated for both core and shell, following a procedure similar to that of Barber and Hill [21]. As a rule of thumb, we have found $N_{\text{g}} = 4n_{\text{ms}}$ to be a good value in all but the most demanding cases (high nonsphericity values, for instance).

The following convention is used. kr_{eq} is the dimensionless equal-volume-sphere size parameter for the whole particle; q is the core/particle size ratio; ε is the eccentricity, or axial ratio, of the particles ($\varepsilon < 1$ for a prolate spheroid; $\varepsilon > 1$ for an oblate spheroid; $\varepsilon = 1$ for a sphere).

3. Results and discussion

In this section we report light scattering results for particles with refractive indices 2.32 + i0.36 for core, 1.2 for shell and 1 for medium. This choice closely corresponds to particles with a hematite core and an yttrium basic carbonate coating, for a vacuum wavelength $\lambda_{\text{o}} = 488$ nm. The accuracy parameter Δ is taken as 10^{-4}. The particles to be studied are randomly oriented spheroids with an equivolume size parameter $kr_{\text{eq}} = 8$ and eccentricities $\varepsilon = 0.6,1$ (spheres) and 1/0.6. This will allow us to compare light scattering properties of particles with equal long-to-short axis ratio both to each other and to their spherical counterpart. In order to find out whether a particular scattering

effect is characteristic of the given size parameter or, on the contrary, can be considered as a more general feature, a second set of calculations has been made for $kr_{eq} = 1$, 5 and 10, and the same ε value; those data are not shown here for brevity.

Figs. 1–6 show all nonzero Müller matrix elements for prolate and oblate spheroidal particles with a 0.6 : 1 axial ratio, as well as those for spheres. For spheres, $F_{22}/F_{11} = 1$ and $F_{33} = F_{44}$. Scattering angle (the angle between the incident and scattered directions, with $\theta = 0$ for unscattered radiation and $\theta = 180^\circ$ for backscattering) and relative core ratio q are plotted in the horizontal axes.

3.1. The matrix element F_{11}

Angular scattering patterns can be seen to be similar for prolate and oblate particles with the same long-to-short axis (Fig. 1). They exhibit some features also seen in earlier works on

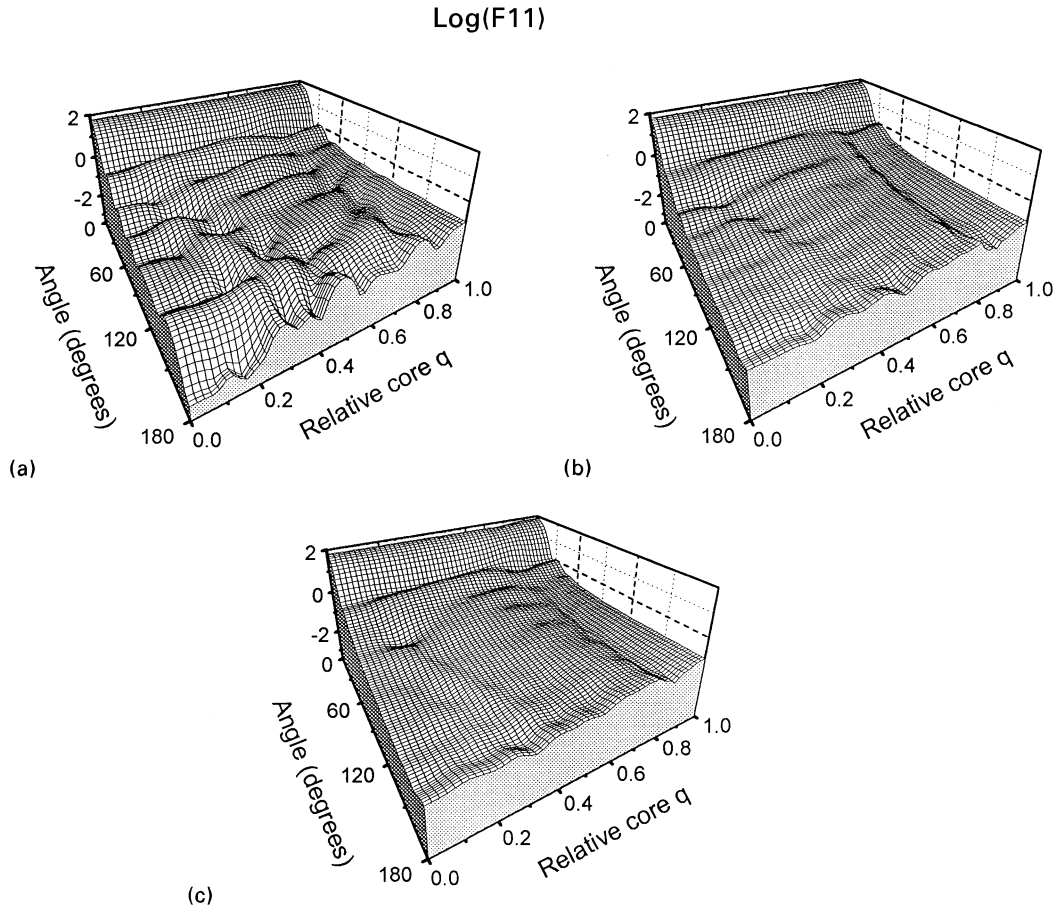

Fig. 1. F_{11} Müller matrix element for an ensemble of (a) coated spheres, and coated, randomly oriented (b) prolate and (c) oblate spheroids, as a function of scattering angle θ and relative core size q. All figures are for a size parameter $kr_{eq} = 8$ and refractive indices 2.32 + i0.36 (core), 1.2 (coating).

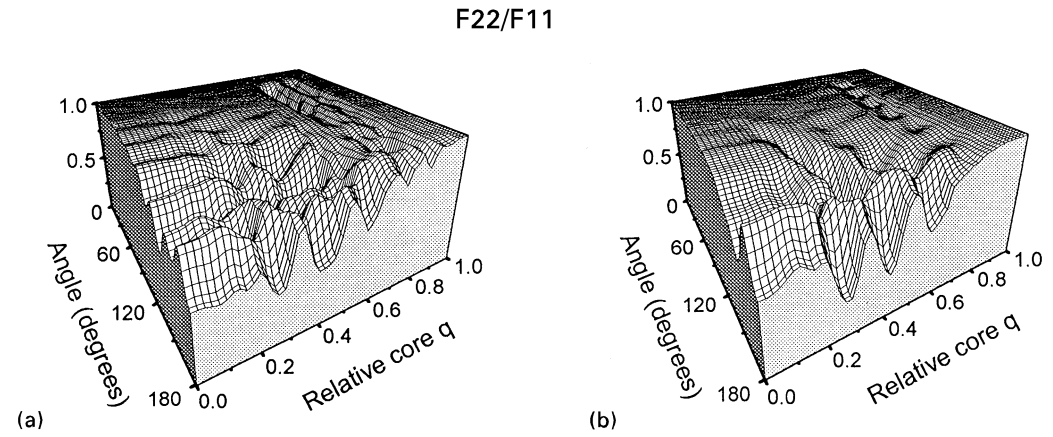

Fig. 2. F_{22}/F_{11} ratio for an ensemble of coated, randomly oriented (a) prolate spheroids, (b) oblate spheroids.

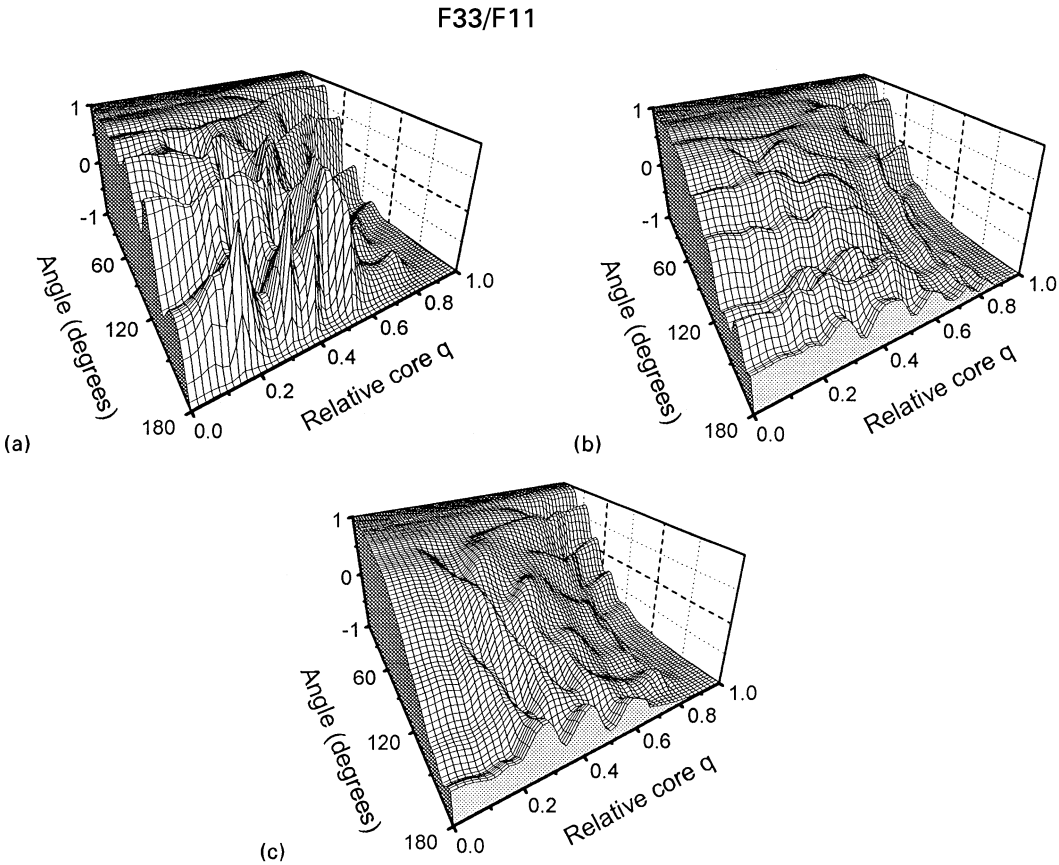

Fig. 3. F_{33}/F_{11} ratio for an ensemble of (a) coated spheres, and coated, randomly oriented (b) prolate and (c) oblate spheroids.

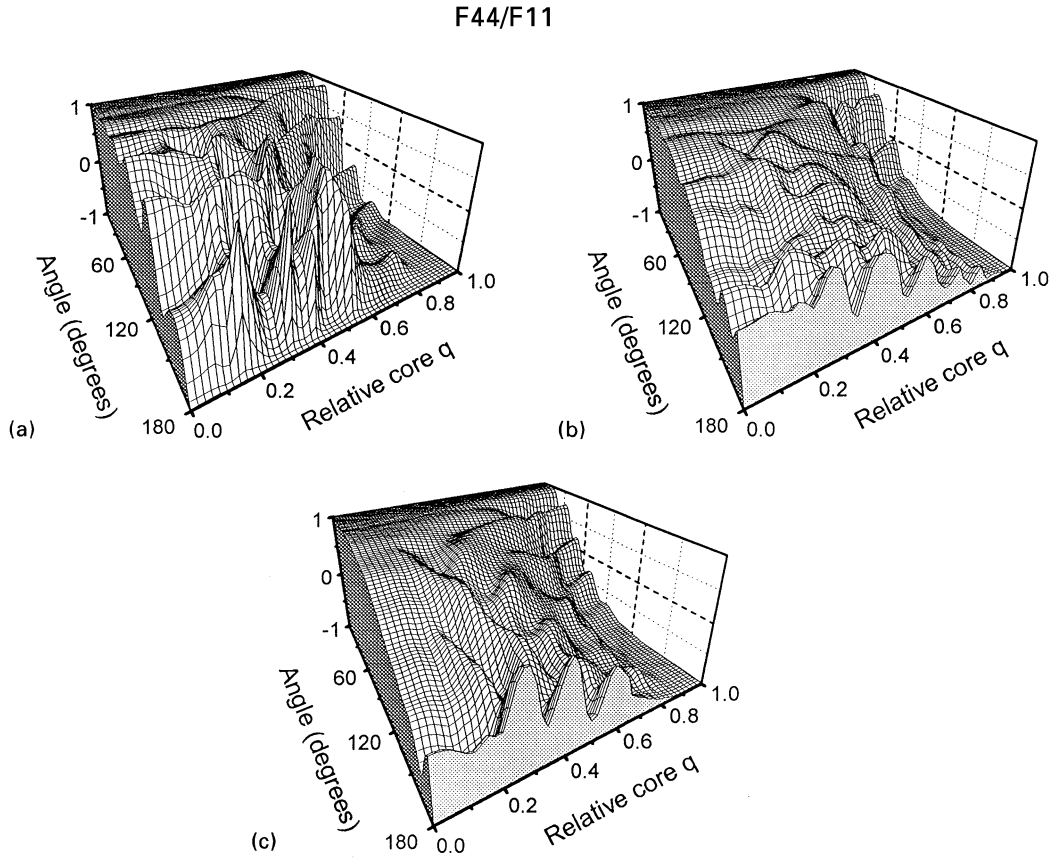

Fig. 4. Same as Fig. 3 for F_{44}/F_{11}.

homogeneous particle systems, such as a similar pattern for low angle values, whatever the particle geometry, as well as the overall similarity of F_{11} for prolate and oblate spheroids [22]. On the other hand, nonspherical particles are not always found to be better scatterers in the backscattering direction. Similarly, our calculations for $kr_{eq} = 1$, 5 and 10 also show that F_{11} is nearly identical for oblate and prolate particles with reciprocal axial ratios, but no general conclusion can be drawn on the backscattering behavior, where spherical particles are only sometimes better scatterers at $\theta = 180^{\circ}$, depending on core and total particle size.

In a more general sense it can be said that F_{11} patterns become smoother for nonspherical particles, showing less rapid variations both for varying θ (core size fixed) and for varying q (at a given angle). This smoothing effect can, in fact, be found to take effect in all Müller matrix elements and for all sizes studied ($kr_{eq} = 1$, 5, 8, 10), being less evident as particles become smaller. In all three figures ($kr_{eq} = 8$, $\varepsilon = 0.6$, 1, 1/0.6), F_{11} is seen to exhibit similar patterns. As a general trend, F_{11} values increase with q for any angle. However, at about $q = 0.7$ the curves reach local maxima, thus giving way to lower values for q between 0.7 and 0.9, and again increasing values for core sizes approaching unity. It is interesting to note that also at $kr_{eq} = 5$ and 10 do $F_{11} - \theta$ curves

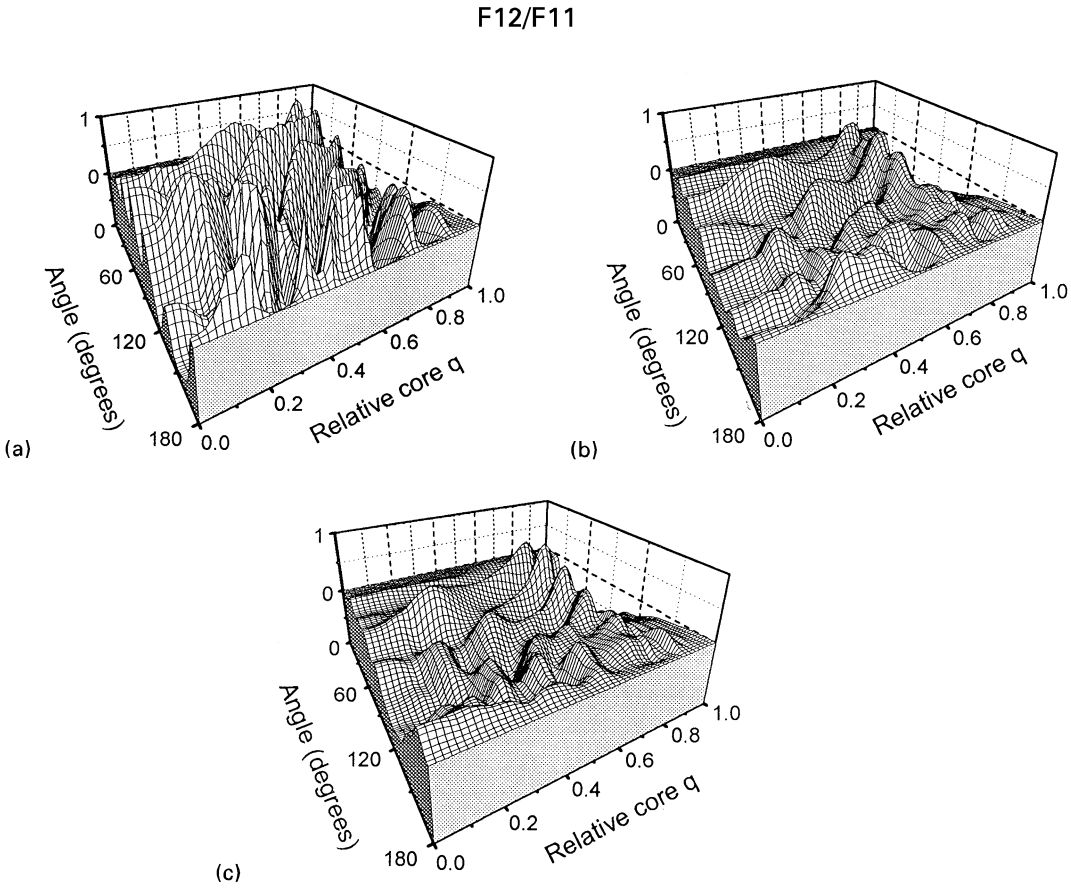

Fig. 5. Same as Fig. 3 for F_{12}/F_{11}.

reach maximum values for a given core size. However, it would be premature to conclude that such a feature occurs for an arbitrary size range. On the other hand, the differences for randomly oriented particles with reciprocal axial ratios are small enough to make difficult a characterization of noneccentricity (oblate/prolate) via F_{11} measurements. The spherical–nonspherical differences will be hard to observe in real laboratory systems, where even a small degree of polydispersity will wipe out the rapidly varying F_{11} patterns.

3.2. The ratio F_{22}/F_{11}

This Müller matrix element is considered as a good indicator of nonsphericity [23], since it is equal to unity for spherical particles. However, although it can substantially deviate from unity, this is not always the case: nonspherical particles can have F_{22}/F_{11} elements close to 1. This fact can erroneously lead to think that unity implies sphericity.

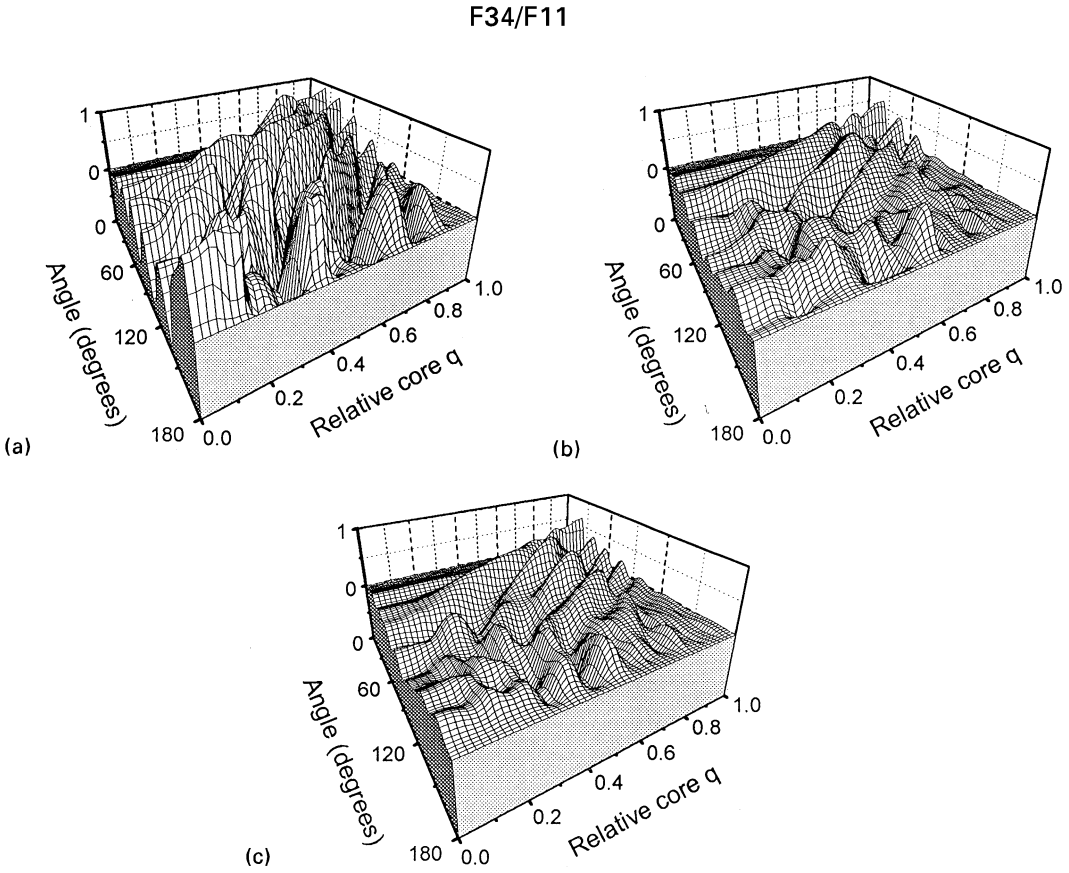

Fig. 6. Same as Fig. 3 for F_{34}/F_{11}.

This can be seen in Fig. 2. Except for a region at $q \sim 0.7$–0.8, all values of F_{22}/F_{11} are very close to unity at angles smaller than about 90° (in fact, oblate particles with a core size larger than 0.9 show F_{22}/F_{11} values higher than 0.99 for *all* angles). When the core size is smaller than 0.6 times the particle size, the behavior of F_{22}/F_{11} vs angle is as follows: first, it gets very close to 1; then, at a certain angle (100–110° for prolate particles, 110–120° for oblate particles), it decreases until it reaches a minimum value at $\theta \sim 140$–$150°$, increases again up to about $\theta \sim 170°$ and has a final decrement at backscattering. The differences between prolate and oblate particles are now more visible. As mentioned above, the ratio departs from unity at lower angles for prolate particles than for oblate ones. It can also be seen that the minima at $\theta \sim 150°$ are deeper for prolate spheroids. This behavior, also observed for $kr_{eq} = 10$, leads us to think that the F_{22}/F_{11} ratio can be used to distinguish prolate and oblate particles of the same volume and axial ratio also in the case of inhomogeneous systems, just as it has been used in the past for homogeneous particles. Particles of a smaller size (data not shown) yield almost complete polarization ($F_{22}/F_{11} \approx 1$), which would make particle sizing more difficult. However, even for $kr_{eq} = 1$, differences between prolate and oblate particles are noticeable when the core size is large enough.

As core size increases, a new feature appears. For prolate spheroids with a $q \sim 0.7$, the F_{22}/F_{11} ratio departs from unity at much smaller angles, and $F_{22}/F_{11} - \theta$ curves show a series of deeper minima than for equivolume oblate spheroids. Furthermore, the maxima and minima observed for lower q in the 150–180° θ range disappear. It is interesting to note that this decrease in F_{22}/F_{11} is located at the same core value region ($q \sim 0.7$) where the local maximum of F_{11} was observed in Fig. 1. This poins to a "transition region" in the $q \sim 0.7$ region, where light scattering properties vs angle behave differently, although this cannot be extrapolated to other size parameters, and thus cannot be considered as a particular feature for a fixed core size (similar behavior is seen for $kr_{eq} = 10$ but not for $kr_{eq} = 5$).

3.3. The ratios F_{33}/F_{11} and F_{44}/F_{11}

Since $F_{33} = F_{44}$ for spheres (Figs. 3a and 4a), any difference between these Müller matrix elements indicates a deviation from sphericity. For all three particle types, the ratios F_{33}/F_{11} (θ,q) plot takes values close to unity for small q and θ values, whereas the behavior is opposite in the high (θ,q) corner, with ratios approaching -1. This is a common feature for all but the smallest particle sizes studied in this work. We cannot always expect this behavior in the general case, not even for this particular size parameter, since it can merely reflect the change in scattering curves from a particle with a large, absorbing material ($q = 0$) to that with a small, nonabsorbing material ($q = 1$). We will therefore focus on the differences between oblate, prolate and spherical particle systems, as well as on the gradual variation of scattering properties as the core size increases.

The most evident distinguishing feature about the ratio F_{33}/F_{11} for a sphere respect to an spheroid (Fig. 3) is its very fast variation when either angle or core size is changed. For any core value, ratio-angle curves show maxima and minima which are both larger in number and more rapidly varying than for spheroidal particles (this behavior is also clearly visible for $kr_{eq} = 10$, present at a smaller scale for $kr_{eq} = 5$, and is absent for $kr_{eq} = 1$). In the side scattering range, $F_{33} > F_{44}$ for $kr_{eq} = 8$ (compare Figs. 3b and 4b, 3c and 4c), as well as for $kr_{eq} = 5{,}10$. The differences between F_{33} and F_{44} are smaller for oblate spheroids, in agreement with the results of Asano and Sato [22] for homogeneous spheroids, and of Mishchenko [23] for homogeneous cylinders.

Differences are also found in the backscattering region, where ratios for oblate and prolate particles are different. While theory yields that $F_{33}/F_{11} = F_{44}/F_{11} = -1$ for spheres at $\theta = 180°$, these ratios have different values for nonspherical particles; for some value of q,F_{44}/F_{11} can even be positive. This suggests that light scattering properties in the backscattering region can be a useful tool for particle sizing, and also agrees with the well-known fact that backscattering is most sensitive to particle shape. We can also see that, for all sizes and shapes studies, $F_{33}/F_{11} \approx F_{44}/F_{11}$ when the core is large ($q > 0.9$).

3.4. The ratio F_{12}/F_{11}

As in all other Müller matrix elements, linear polarization (other authors define it as minus F_{12}/F_{11}) show faster variations with both core and angle in the case of spherical particles (compare Fig. 5a–c). For spheres, θ–q plots yield a set of oblique polarization strips, so that a particular maximum (or minimum) is attained at decreasing angle values as core size increases. For all but the

smallest and largest values of q, angular scattering curves show extreme values of polarization, both positive and negative.

For nonspherical particles, polarization values do not reach the extremes (± 1). Minimum polarization values are found for an angular range centered at about 120°, when core values are small, and about 60°, when core values are large. But, unlike the smaller particles, where a polarization miminum can be found at intermediate angle for any core value, nonspherical particles with $kr_{eq} = 8$ and 10 have positive polarization values for a range or core sizes. When q approaches 0.7, polarization-angle curves have positive values; for oblate particles, such curves have more local maxima and minima, specially at angles less that 90°.

Asano's results [22] about the degree of polarization being close to that of the equivolume spheres for small scattering angles are also found for coated spheroids. However, our data for $kr_{eq} = 8$ show that they only hold for small angles ($\theta < 30°$). Data from other particle sizes indicate that the angle range of spherical–nonspherical coincidence gets smaller for larger size parameters ($\theta < 60°$ for $kr_{eq} = 5$, $\theta < 15°$ for $kr_{eq} = 10$).

3.5. The ratio F_{34}/F_{11}

Several features are common for F_{34}/F_{11} (Fig. 6) and F_{12}/F_{11} (Fig. 5). As in the case of linear polarization, the ratio F_{34}/F_{11} is more strongly core- and angle-dependent for spheres than for spheroids. When particles are nonspherical, this ratio does not reach extreme values (± 1). This feature, also found for $kr_{eq} = 1, 5, 10$ suggests that F_{34}/F_{11} values close to plus or minus one might be a hint of particle nonsphericity in the general case. This has also been observed by Kuik [24] for monodisperse, randomly oriented ensembles of spheroids and cylinders with a dimension ratio (long-to-short axis, or diameter-to-length) as high as 7. The maximum values of F_{34}/F_{11} can be seen to reside in the region of $q = 0.6$–0.8 for angles less than about 100°. In the forward and backward scattering regions, this ratio, like F_{12}/F_{11}, is close to zero (being identically zero for $\theta = 0°$,180°, as predicted by the theory). F_{34}/F_{11} is also seen to be similar for spheres and nonspheres up to a certain angle; again, this angle is smaller as the size parameter grows larger.

4. Concluding remarks

We have presented computed results on light scattering and polarization properties for some particle systems of spheroids on random orientation using the T-matrix method [3] as modified by Peterson and Ström [7,8]. All six nonzero Müller matrix elements have been calculated and presented; together with scattering and extinction cross sections, they yield all the information available on static light scattering by a volume element. We cannot draw general conclusions due to the large number of parameters involved, not only particle size and shape, but also core size and composition; our aim was to show light scattering differences (respective to a sphere) when an inner core exists and has to be taken into account

The well-known fact that the EBCM can be ill-conditioned for particles with large size and/or deviation from eccentricity is enhanced by the structure of the T matrix for coated particles; this comes mainly from the $\mathbf{AA}_2$ matrix (Eq. (3)) whose elements depend on the product of two Hankel functions and can therefore can reach very high values. Several checks have been made to ensure

data quality. Some inequalities between the elements of the Müller matrix have been used for checking purposes at all angle values [25]. Calculations for spheres have been compared to data obtained from another, independently developed computer code based on the Aden-Kerker theory for coated spherical particles [2,26]. For the case of spheroids, comparisons with respect to the homogeneous T-matrix theory were made by making equal both core and coating refractive index, as well as by making $m_{\text{shell}} = 1$. When both refractive indices are made nonabsorbing (no imaginary part), scattering and extinction cross sections coincide.

The data showed in the present paper, plus those used for checking purposes ($kr_{\text{eq}} = 1, 5, 10$) represent calculations for a total of 204 particle types in random orientation, with a total CPU usage of 5.1 h on a Pentium computer (200 MHz, 32 Mbyte RAM). In spite of the large number of particles, we should stress that they only represent a minimum fraction of all possible compositions of particle size, shape, and composition. Future works should address particles of other shapes, such as cylinders. An interesting field of study is that of concave particles. All light scattering studies of coated particles have been focused on spheres or spheroids, and no data exist on inhomogeneous convex bodies, whose behavior can be significantly different to those of equivalent-volume concave ones. Chebyshev particles, such as those used by Wiscombe [27], would provide adequate checking particles.

Acknowledgements

Financial support for this research was provided by DGICYT, Spain (Proj. - PB94-0812-C02-1).

References

[1] Mie G. Ann d Phys 1908;25:377.
[2] Aden AL, Kerker M. J Appl Phys 1951;22:1242.
[3] Waterman PC. Phys Rev D 1971;3:825.
[4] Barber PW. IEEE MTT 1977;25:373.
[5] Mishchenko MI. J Opt Soc Am A 1991;8:871; Mishchenko, MI, J Opt Soc Am A 1992;9:497.
[6] Mishchenko MI, Travis LD, Mackowski DW. JQSRT 1996;55:535.
[7] Peterson B, Ström S. Phys Rev D 1974;10:2670.
[8] Ström S. Phys Rev D 1974;10:2685.
[9] Wang DS, Chen HCH, Barber PW, Wyatt PJ. Appl Opt 1979;18:2672.
[10] Asano S, Yamamoto G. Appl Opt 1975;14:29.
[11] Al-Rizzo HM, Tranquilla JM. J Comp Phys 1995;119:342.
[12] Al-Rizzo HM, Tranquilla JM. J Comp Phys 1995;119:356.
[13] Farafonov VG, Voshchinnikov NV, Somsikov VV. Appl Opt 1996;35:5412.
[14] Ohmori M, Matijevic E. J Coll Int Sci 1993;160:288.
[15] Bohren CB, Huffman DR. Absorption and scattering of light by small particles. New York: Wiley, 1983.
[16] Siewert CE. Astrophys J 1981;245:1080.
[17] Hovenier JW, van der Mee CVM. Astron Astrophys 1983;128:1.
[18] Stratton JA. Electromagnetic theory. New York: McGraw-Hill, 1941.
[19] Tsang LT, Kong JA, Shin RT. Radio Sci 1984;19:629.
[20] Mackowski DW, Altenkirch RA, Menguc MP. Appl Opt 1990;29:1551.
[21] Barber PW, Hill SC. 1990. Light scattering by particles: computational methods. Singapore: World Scientific, 1990.

[22] Asano S, Sato M. Appl Opt 1980;19:962.
[23] Mishchenko MI, Travis LD, Macke A. Appl Opt 1996;35:4927.
[24] Kuik F. Single scattering of light by ensembles of particles with various shapes, Ph.D. Thesis, University of Amsterdam, 1992.
[25] Fry ES, Kattawar GW. Appl Opt 1981;20:2811.
[26] Quirantes A, Delgado AV. J Phys D 1997;30:2123.
[27] Wiscombe WJ, Mugnai A. NASA Ref Publ 1157, NASA/GSFC, Greenbelt MD, 1986.